Environmental Pollution 232 (2018) 580–590

Contents lists available at ScienceDirect

Environmental Pollution

journal homepage: www.elsevier.com/locate/envpol

Photocatalysis of bisphenol A by an easy-settling titania/titanate composite: Effects of water chemistry factors, degradation pathway and theoretical calculation☆

Xiao Zhao [a, b], Penghui Du [c], Zhengqing Cai [d], Ting Wang [a], Jie Fu [d, *], Wen Liu [a, c, **]

[a] College of Environmental Sciences and Engineering, Peking University, The Key Laboratory of Water and Sediment Sciences, Ministry of Education, 100871, China
[b] Center for Agricultural Water Research in China, China Agricultural University, Beijing 100083, China
[c] School of Civil and Environmental Engineering, Georgia Institute of Technology, Atlanta, GA 30332, United States
[d] Department of Environmental Science & Engineering, Fudan University, Shanghai, 200433, PR China

ARTICLE INFO

Article history:
Received 3 April 2017
Received in revised form
24 September 2017
Accepted 28 September 2017
Available online 6 October 2017

Keywords:
Titanate nanotubes
TiO_2
Photocatalysis
Bisphenol A
Easy-setting
DFT calculation

ABSTRACT

Bisphenol A (BPA) is a widely concerned endocrine disrupting chemical and hard to be removed through conventional wastewater treatment processes. In this study, we developed a TiO_2 decorated titanate nanotubes composite (TiO_2/TNTs) and used for photocatalytic degradation of BPA. TEM and XRD analysis show that the TiO_2/TNTs is a nano-composite of anatase and titanate, with anatase acting as the primary photocatalytic site and titanate as the skeleton. TiO_2/TNTs exhibited excellent photocatalytic reactivity and its easy-settling property leaded to good reusability. After 5 reuse cycles, TiO_2/TNTs also could photodegrade 91.2% of BPA with a high rate constant (k_1) of 0.039 min^{-1}, which was much better than TiO_2 and TNTs. Higher pH facilitated photocatalysis due to more reactive oxygen species produced and less material aggregation. The presence of NaCl and $CaCl_2$ showed negligible effects on BPA degradation, but $NaHCO_3$ caused an inhibition effect resulting from consumption of ·OH. Humic acid inhibited degradation mainly due to blockage of the active sites of TiO_2/TNTs. Degradation pathway was well interpreted through theoretical calculation. Hydroxyl radical played the dominate role in BPA photodegradation, and the atoms of BPA with high Fukui index based on density-functional theory (DFT) calculation are the radical easy-attacking (f^0) sites. Considering the good photocatalytic reactivity, reusability, stability and settle property, TiO_2/TNTs promises to be an efficient alternative for removal of organic compounds from wastewaters.

1. Introduction

Natural waters are threatened by a variety of emerging pollutants now. Among numerous persistent organic chemicals, endocrine disrupting chemicals (EDCs) has aroused the public concerns in recent years (Rogers et al., 2013; Vandenberg et al., 2012). Bisphenol A (BPA) is one of the most extensively studied EDCs for its wide use in plastic industry and acute toxicity (Fromme et al., 2002; Lombó et al., 2015; Rogers et al., 2013). Triggered by the risk concern, the predicted no-effect concentration (PNEC) of BPA has been lowered from 100 to 0.06 μg/L (Wright-Walters et al., 2011). BPA is ubiquitous in environment and can be found in landfill leachates, air, dust and waters with concentrations higher than PNEC values (Flint et al., 2012). In addition, BPA has an estimated half-life of 160 days in natural waters (Staples et al., 1998), so typical wastewater treatment plants using activated sludge or carbon adsorption are inefficient in removing BPA (Gültekin and Ince, 2007; Zhang and Zhou, 2008).

Advanced oxidation processes, especially photocatalytic degradation, are promising approaches for removing BPA from wastewater treatment plants or surface waters (Akbari et al., 2016; Gültekin and Ince, 2007; Guo et al., 2009; Kondrakov et al., 2014). Titanium materials have attracted much attention as the candidates

☆ This paper has been recommended for acceptance by Dr. Harmon Sarah Michele.

* Corresponding author.
** Corresponding author. College of Environmental Sciences and Engineering, Peking University, The Key Laboratory of Water and Sediment Sciences, Ministry of Education, 100871, China.
E-mail addresses: jiefu@fudan.edu.cn (J. Fu), wen.liu@pku.edu.cn (W. Liu).

https://doi.org/10.1016/j.envpol.2017.09.094
0269-7491/

of appropriate photocatalysts. TiO_2 nanoparticle is an effective photocatalyst for BPA degradation (Ohko et al., 2001; Tsai et al., 2009; Wu et al., 2016), however the difficulty of separation and recovery of this nanoparticle limits its practical application (Guo et al., 2009; Liu et al., 2013a). Surface/morphology modification (Guo et al., 2009) or use of supports (Fukahori et al., 2003b) can greatly facilitate the separation for Ti-based nanomaterials.

One-dimensional titanate nanotube (TNT) derived from TiO_2 is an excellent adsorbent for metal cations (Liu et al., 2013b; Sheng et al., 2011) and also a good support for catalysts (Doong and Liao, 2016; Zhao et al., 2016a). Despite of its large specific surface area, TNTs has low photocatalytic reactivity under neither UV nor solar illumination, mainly because of the rapid electron-hole recombination rate (Lee et al., 2007; Yu et al., 2006a). Surface modification through doping metals can greatly enhance either photocatalytic reactivity or sedimentation of the materials (Chen et al., 2013; Grandcolas et al., 2013; Liu et al., 2015; Zhao et al., 2016a). Decorating nano-TiO_2 onto the TNTs holds the promise to combine the benefits of large surface area of TNTs and the great photocatalytic activity of TiO_2 (Yu et al., 2007; Zhu et al., 2004). Compared to other conventional supports (such as activated carbon, SiO_2, Al_2O_3 and resin) (Anderson and Bard, 1997; Cai et al., 2013; Mutin et al., 2004; Torimoto et al., 1997), TNTs are good supports for TiO_2 considering the following advantages. Firstly, TiO_2 and TNTs are both Ti-nanomaterials, titanate is derived from TiO_2 through hydrothermal treatment while it also can convert to TiO_2 via calcination (Bavykin and Walsh, 2010; Yu et al., 2007; Zhu et al., 2004). Therefore "homogeneity" of TiO_2 and TNT can achieve easy phase transformation from each other. Secondly, TNTs are multi-layered nanotubes with fine structure and specific shape (Bavykin and Walsh, 2010; Chen et al., 2002; Liu et al., 2013b). Coating TiO_2 onto the TNTs with large specific surface area can enhance the overall photocatalytic reactivity of the composite material, and expose lots of nano-scale reactive sites when reacting with contaminants. Thirdly, excellent ion-exchange performance of TNTs can efficiently capture Ti^{4+} when decorated TiO_2 through sol-gel method, and also can retard the adverse effects of metal cations (e.g., Na^+ and Ca^{2+}) on reaction (Liu et al., 2013b; Sun and Li, 2003). Finally, good sedimentation property of TNTs ensures easy separation of the material after application (Liu et al., 2013a).

However, fundamental water chemistry associated with the photolysis of BPA with the TiO_2 decorated TNTs (abbreviated to TiO_2/TNTs) remain unexplored. Key information includes the effects of pH, coexisting ions and natural organic matter (NOM), along with the materials recyclability and the underlying degradation mechanisms. The generation of radicals, ionization state, and agglomeration behavior of contaminants or photocatalysts in solution systems are highly pH-dependent (Akpan and Hameed, 2009; Konstantinou and Albanis, 2004). The influence of commonly detected ions, e.g., Na^+, Ca^{2+} and HCO_3^-, are also of research interest. NOM ubiquitously exists in groundwater with concentrations ranged from 0.5 to >20 mg/L as total organic carbon (TOC) (Thurman, 2012). NOM can significantly impact the surface, transport and fate of nanomaterials and some organic contaminants (Wu et al., 2016; Zhao et al., 2016b). Likewise, such conditions may affect BPA photodegradation and need to be further studied.

In addition, knowledge on the BPA degradation mechanism, especially structural information on aromatic products of BPA photocatalytic degradation is limited (Kondrakov et al., 2014). It is of high importance and interest to reveal the relations between BPA properties and photocatalyst activity. Theoretical calculation, especially the development of density-functional theory (DFT), provides a new tool for exploring the interaction between material and pollutants, or reaction mechanisms in typical processes (e.g., photocatalysis) (Di Valentin et al., 2008; Wei et al., 2017; Zhao and Liu, 2007). Therefore, theoretical calculation on photocatalysis of BPA will present new sights for better understanding the underlying mechanisms.

With consideration the challenges in photocatalytic water treatment area, such as energy-saving, material recovery, and high radicals yield efficiency (Cates, 2017), the developed photocatalysts are expected to have some specific characteristics. Firstly, the photocatalysts should show high photocatalytic activity, which has high radicals (e.g., ·OH) yield so as to efficiently attack contaminants; Secondly, the photocatalysts should be able to easily separated from waters and reused so as to reduce application cost; Thirdly, the photocatalysts should present high reactivity even in complex water matrix; Finally, degradation mechanisms for different contaminants should be explored so as to better design/modify photocatalysts. Given the above context, we have developed a composite material (TiO_2/TNTs) of good practical application potential, which was used for photocatalytic removal of BPA. In this study, the developed materials have all the merits mentioned above and BPA degradation mechanism was clearly investigated. The specific objectives of this work were to: (1) synthesize an effective and reusable TiO_2/TNTs for BPA removal under UV light; (2) test the effects of typical water chemistry parameters on photocatalysis, including pH, coexisting ions and humic acid (HA); (3) explore the degradation pathway of BPA; and (4) interpret the underlying mechanism on BPA attacking by radicals in the photocatalysis process by means of DFT calculation.

2. Methods and materials

2.1. Chemicals and materials

TiO_2 (P25, ca. 80% of anatase and 20% of rutile) was supplied from Degussa (now Evonik) of Germany. *Tetra-butyl* titanate ($Ti(OBu)_4$, >98%) was obtained from Strem Chemicals of USA. NaOH (GR grade), NaCl, $CaCl_2$, $NaHCO_3$, KI, isopropanol and *p*-benzoquinone (BQ) were all purchased from Acros Organics (Fair Lawn, NJ, USA). Deionized (DI) water (Millipore Co., 18.2 MΩ cm) was used to prepare all solutions. Humic acid (Sigma-Aldrich, St. Louis, MO, USA) was used as the model NOM. BPA (Acros Organic, USA, properties shown in Table S1) was dissolved into methanol (HPLC grade, BDH, USA) to form a stock solution of 1 g/L, and diluted properly for further use.

2.2. Synthesis and characterizations of TiO_2/TNTs

Firstly, TNTs were prepared through an alkaline hydrothermal method as described by Xiong et al. (2010). Specifically, TiO_2 nanoparticles were dispersed into 10 M NaOH solution and magnetically stirred for 12 h. Afterwards, the mixture was transferred into a Teflon reactor with a stainless cover, and then heated at 130 °C for 72 h. When cooled down to ambient temperature, the white precipitates were washed with DI water to neutral and then dried at 80 °C for 4 h.

TiO_2/TNTs were then synthesized through a sol-gel method. 2.13 mL *tetra-butyl* titanate was added into 21.0 mL absolute alcohol (in a 100 mL beaker) with stirring for 10 min. 0.2 g TNTs was then added into the mixture and stirred for another 10 min, followed by an addition of 0.188 mL concentrated HCl. After 1 h of stirring, 1 mL of deionized water was added dropwise for hydrolysis, and after another 2 h of stirring, the milk-like mixture was centrifuged at 10000 rpm for 10 min. The obtained precipitates were washed with absolute ethanol twice and deionized water three times. Finally, the products were dried at 80 °C for 4 h firstly and then calcined at 400 °C in a muffle furnace for 3 h.

Details on characterization methods of TiO_2/TNTs are shown in Supplementary data (M1).

2.3. Photocatalysis of BPA

Photocatalytic experiments were conducted in a cuboid quartz reactor with a total volume of 300 mL (5 × 5 × 12 cm) under UV light, which was supplied by a high-pressure mercury lamp (150 W, 365 nm). The light was placed beside the reactor (10 cm away) with cooling air supplied to maintain the system temperature of 25 ± 0.5 °C. The UV light density at 365 nm in the reactor center was determined as 2.5 mW/cm^2. Fig. S1 gives the illumination spectra of the UV lamp, which was measured by a Newport model 1916-R optical power meter.

A continuous photocatalysis tests were firstly designed for comparison on photocatalytic activities of TiO_2/TNTs, precursor TiO_2 and TNTs. The reaction was initialized with addition of 5 mg/L of BPA and 0.2 g/L photocatalyst at pH 7. After 1 h's reaction, the material was separated through gravity settling, which was lasted for 6 h. The supernate was removed and the precipitate (material) was further reused for BPA degradation with initial concentration of 5 mg/L at pH 7. The material reuse was lasted for 5 cycles and BPA degradation kinetic was investigated in each cycle. In addition, photocatalytic degradation of BPA at low concentration of 200 μg/L was also evaluated at identical conditions.

Four scenarios were investigated for the effects of water chemistry factors on photocatalytic degradation of BPA: (1) To test the effect of material dosage, TiO_2/TNTs dosage was varied from 0.05 to 0.8 g/L with initial BPA concentration of 5 mg/L at pH 7; (2) To test the effect of pH, solution pH was adjust from 3 to 11 using diluted HCl and NaOH, and TiO_2/TNTs dosage was 0.2 g/L with initial BPA concentration of 5 mg/L; (3) To test the effect of conventional ions, 5 mmol/L NaCl, $CaCl_2$ and $NaHCO_3$ was added, respectively; (4) To test the effect of HA, HA concentration was varied as 0–10 mg/L (as TOC), material dosage was 0.2 g/L while initial BPA concentration was 5 mg/L at pH 7. Adsorption of HA at various concentrations by TiO_2/TNTs was also studied at identical conditions, and HA adsorption kinetics were firstly examined lasting for 180 min. HA concentrations before and after adsorption were measured as TOC on a VCPN TOC-analyser (Shimadzu, Japan).

Samples were taken at specific time intervals, and then immediately centrifuged (8000 rpm, 3 min) and supernatant was filtered through a 0.22 μm polytetrafluoroethylene (PTFE) membrane. BPA concentration in the aqueous phase was determined using an Agilent 1100 high performance liquid chromatography (HPLC) equipped with a Zorbax RX-C18 column (2.1 × 150 mm, 5 μm). Mobile phase was run as mixture of methanol and water at 60:40 (v/v) and a flow rate of 0.2 mL/min in the isocratic mode, and the eluate was analyzed with a UV diode array detector at 220 nm. TOC of the sample during the photocatalysis was also determined using a VCPN TOC-analyser (Shimadzu, Japan) to investigate BPA memorization efficiency.

First-order kinetic model simplified from Langmuir-Hinshelwood (L-H) model was introduced to describe the photocatalysis reaction (Liu et al., 2014; Satterfield, 1970):

$$\ln(C0/Ct) = k_1 t \tag{1}$$

in which C_0 and C_t (mg/L) are the BPA concentrations at initial and time t (min), respectively, and k_1 (min^{-1}) is the first-order apparent rate constant.

All the photocatalytic experiments are conducted in duplicate. Data were plotted as mean of duplicates, and error bars were calculated as standard deviations, indicating the data reproducibility. Statistical significance testing of calculated values was performed by means of ANOVA t-test using SPSS (SPSS 14.0, Chicago, Illinois, USA).

2.4. Identification of degradation products

BPA degradation products were determined on a high performance liquid chromatography-mass system (HPLC-MS, HP 1100 LC-MS^n Trap SL System, Agilent, USA) with a Zorbax RX-C18 column. Details on LC-MS operation conditions are shown in Supplementary data (M2 and Table S2).

2.5. Computational calculation theories and methods

All of the computations were performed based on DFT method using a Gaussian 03 package (Frisch et al., 2003). Geometry optimization and sing-point (SP) energy calculation were executed using the hybrid B3LYP method, which combines Hartree, Fock and Becke exchange terms with the Lee-Yang-Parr correlation function. And a 6–31* basis set was used.

For the DFT reactivity descriptor calculations, Fukui function is an important concept in conceptual density functional theory, which has been widely used in prediction of reactive site of electrophilic, nucleophilic, and radical attacks (Parr and Yang, 1984). Fukui function is defined as:

$$f(r) = \left(\frac{\partial^2 E}{\partial N.\,\partial v(r)}\right) = \left[\frac{\partial \mu}{\partial v(r)}\right]_N = \left[\frac{\partial \rho(\mathrm{r})}{\partial N}\right]_{V(r)} \tag{2}$$

where $\rho(r)$ is the electron density at a point r in space, N is electron number in present system, and the constant term v in the partial derivative is external potential. In the condensed version of Fukui function, atomic population number is used to represent the amount of electron density distribution around an atom. The condensed Fukui function can be calculated unambiguously for three situations:

$$\text{Nucleophilic attack}: f_k^+ = q_N^k - q_{N+1}^k \tag{3}$$

$$\text{Electrophilic attack}: f_k^- = q_{N-1}^k - q_N^k \tag{4}$$

$$\text{Radical attack}: f_k^0 = \left(q_{N-1}^k - q_{N+1}^k\right)/2 \tag{5}$$

where q^k is the atom charge population of atom k at corresponding state. The Fukui function contains relative information about different sites of one molecule, and the reactive sites usually have larger value of condensed Fukui function (CFF) than other regions.

3. Results and discussion

3.1. Characterizations of TiO_2/TNTs

Fig. 1 shows the transmission electron microscopy (TEM) images of various titanium materials. In accordance with the previous studies (Liu et al., 2013b; Xiong et al., 2010; Zhao et al., 2016a), TiO_2 (P25) nanoparticles exhibit as nanospheres with diameters of 20–50 nm (Fig. 1a). After hydrothermal treatment, multilayered titanate nanotubes are formed, with an inner diameter of ca. 4.5 nm and outer diameter of 9 nm (Fig. 1b). The interlayer distance of TNTs was 0.75 nm, which is consistent with the crystal plane of titanate (020) (Chen et al., 2002). For TiO_2/TNTs, TNTs are broken with a decreased interlayer distance of 0.69 nm (Fig. 1c and d), due to damage of tubular structure and conversion of titanate to TiO_2 in the calcination process (Lee et al., 2007; Yu et al., 2006b). More importantly, small particles with diameters of 2–3 nm coated onto TNTs (Fig. 1d), which is anatase according to further X-ray diffraction (XRD) analysis. Energy dispersive X-Ray spectra (EDS) analysis

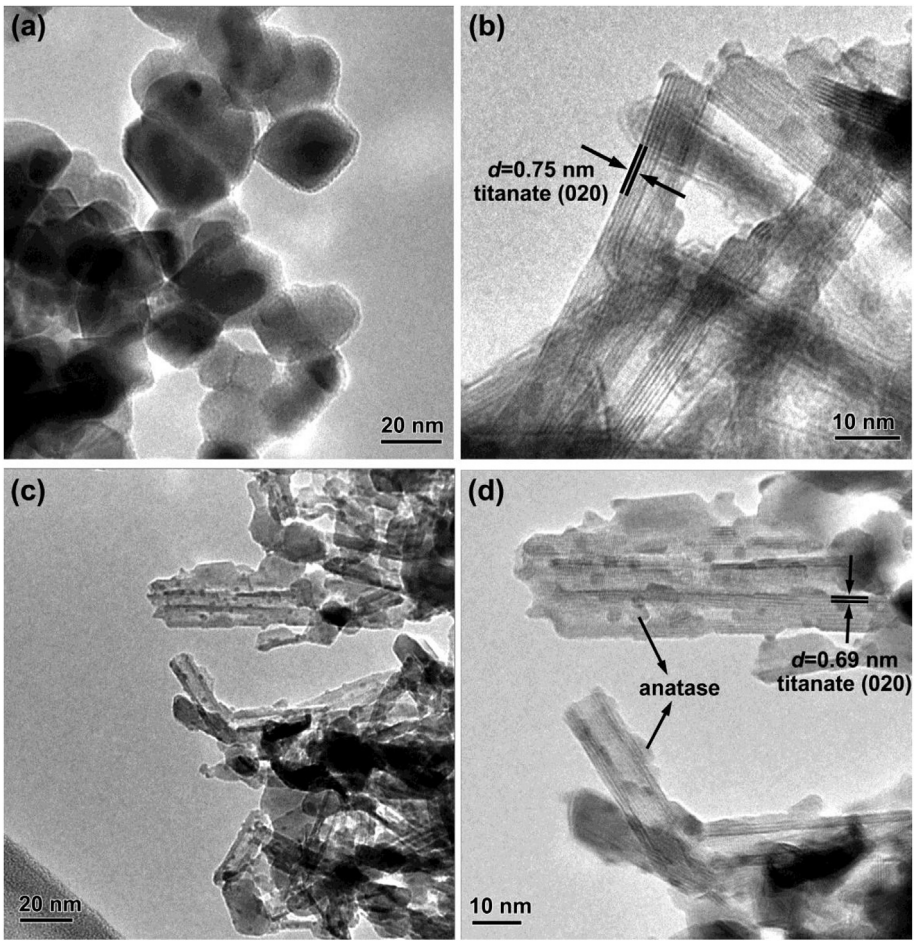

Fig. 1. TEM images of **(a)** P25, **(b)** TNTs, **(c)** and **(d)** TiO_2/TNTs.

indicates that the main elements of TiO_2/TNTs are Na, O and Ti (Fig. S2), suggesting formation of sodium titanate.

Fig. 2 displays XRD patterns of different materials. TiO_2 P25 exhibits as mixed crystal phases of anatase and rutile. After hydrothermal treatment for TNTs synthesis, all the TiO_2 converts to titanate. In addition, the obtained material is a kind of sodium tri-titanate, with chemical formula of $Na_xH_{2-x}Ti_3O_7$ (in which $x = 0–0.75$, depending on the remaining sodium content) (Liu et al., 2013b; Sun and Li, 2003). The tri-titanate composes of layered corrugated ribbons formed through edge-sharing of triple [TiO_6] octahedrons as its skeletal structure and H^+/Na^+ located in interlayers (Liu et al., 2013b; Sun and Li, 2003). The peak at 9.5° represents the interlayer distance of TNTs (Liu et al., 2013b; Sun and Li, 2003). TiO_2/TNTs present both crystal phases of TiO_2 and titanate. However, only the titanate peaks at 9.7° and 28.0° remain, and the interlayer peak greatly decreased due to damage of tubular structure via calcination. Moreover, part of titanate converted to anatase at high temperature. All the TiO_2 attached are found to be anatase, which shows high photocatalytic activity under UV light.

TNTs (272 m^2/g) exhibited much larger Brunauer-Emmett-Teller (BET) specific surface area than P25 (47 m^2/g) (Table S3) (Liu et al., 2014), resulting from its multilayered tubular structure (Bavykin et al., 2006; Xiong et al., 2010). After anatase deposition and calcination for TiO_2/TNTs, the BET surface area decreases to 187 m^2/g, due to damage of the nanotubes as shown in Fig. 1c and d. For both TNTs and TiO_2/TNTs, the N_2 adsorption-desorption isotherms fitted type IV isotherms with H3 hysteresis loops according to BDDT classification (Fig. S3a) (Brunauer et al., 1940), suggesting the presence of mesopores (2–50 nm) in the material. The single point total pore volume of TiO_2/TNTs (0.85 cm^3/g) was also lower than that of TNTs (1.26 cm^3/g), and proportion of small pores (2–3 nm) remarkably decreased for TiO_2/TNTs (Fig. S3b), because deposited

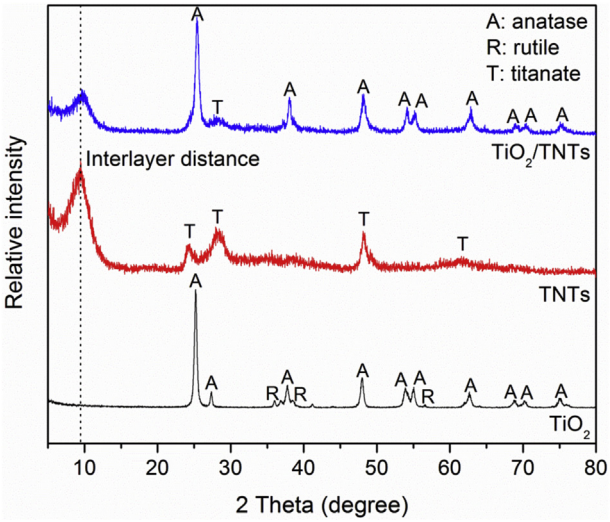

Fig. 2. XRD patterns of various titanium materials.

anatase nanoparticles blocked into the nanotubes and tubes damaged during calcination. The detected point of zero charge (pH_{PZC}) of TiO_2/TNTs (2.93) was close to that of TNTs (2.56) (Fig. S4), but much lower than that of P25 (6.67) (Liu et al., 2014), as still abundant of −ONa/OH groups were located on calcined TNTs.

3.2. Comparison on photocatalytic degradation of BPA by TNTs and TiO_2/TNTs

Fig. 3 compares the photocatalytic degradation kinetics of BPA by different photocatalysts over 5 continuous cycles, and Table S4 lists the simulated first-order kinetic model parameters. Less than 5% of BPA uptake was found in the dark for the all the materials based on adsorption tests. TNTs showed almost no photocatalytic activity toward BPA under UV light, with a low k_1 of 0.001 min^{-1} and a total removal of 5.8% at 60 min even in the first cycle. TiO_2 (P25) showed good photocatalytic activity, with a high k_1 of 0.0849 min^{-1} and removal efficiency of 100% at 60 min in the first cycle. However, due to hard settling of TiO_2 (Fig. S5), >93% of TiO_2 NPs will lose after gravity settling and can not be reused in the next cycle, resulting in dramatic decrease on k_1 (only 0.0003 min^{-1} in the 5th cycle). Only 2.0% of BPA could be removed after 5 cycles by TiO_2. It is quite different for TiO_2/TNTs considering its excellent sedimentation property, as 95.8% of the material could be separated after 6 h' gravity-settling (Fig. S5). Although slightly lower of BPA removal efficiency (94.4%) was observered in the first cycle compared to TiO_2, reusability of TiO_2/TNTs was pretty good. Even in the 5th cycle, the k_1 value was still as high as 0.0394 min^{-1} and 91.2% of BPA could be degraded. In addition, <2% of Ti was dissolved into the solution in the total 5 runs, indicating good stability of TiO_2/TNTs. Therefore, TiO_2/TNTs is a much more promising material compared to TiO_2 NPs for practical application, which will greatly reduce the commercial and energy costs.

TiO_2/TNTs also showed a high removal efficiency for BPA at low concentration of 200 μg/L, and almost all (>99%) of BPA could be degraded within 30 min (Fig. 4). Therefore, TiO_2/TNTs presented a great application potential for removal of such micropollutants in wastewaters, which are usually at ppb level concentration (Fromme et al., 2002; Lombó et al., 2015; Rogers et al., 2013; Vandenberg et al., 2012). Moreover, 66.9% and 100% of TOC was eliminated at BPA concentration of 5 mg/L and 200 μg/L respectively, indicating the high mineralization efficiency during photocatalysis. The BPA degradation and mineralization pathway will be discussed in detail in Section 3.5.

In a typical photocatalysis process for degradation of BPA by TiO_2/TNTs, TiO_2 (anatase) will be excited under UV light, and generates electrons (e^-) in the conduction band and hole (h^+) in the valence band (Eq. (2)) (Akpan and Hameed, 2009; Guo et al., 2009; Zhao et al., 2016a). Subsequently, molecular oxygen and water will accept the electrons and holes to produce reactive oxygen species (ROS) (Eqs. (6)–(10)) (Akpan and Hameed, 2009; Guo et al., 2009; Zhao et al., 2016a). BPA will be further attacked by ROS (Eq. (11)).

$$TiO_2 + h\nu \rightarrow TiO_2^* (e^- - h^+) \quad (6)$$

$$O_2 + e^- \rightarrow \cdot O_2^- \quad (7)$$

$$H_2O + h^+ \rightarrow \cdot OH + H^+ \quad (8)$$

$$\cdot O_2^- + 2H^+ + e^- \rightarrow H_2O_2 \quad (9)$$

$$H_2O_2 + \cdot O_2^- \rightarrow \cdot OH + OH^- + O_2 \quad (10)$$

$$BPA + ROS\ (\cdot OH,\ \cdot O_2^-\ \text{and}\ H_2O_2) \rightarrow \text{intermediates} \rightarrow CO_2 + H_2O \quad (11)$$

TNTs exhibit negligible photocatalytic reactivity, due to the rapid electron-hole recombination rate after excitation (Lee et al., 2007; Yu et al., 2006a). While for TiO_2/TNTs, the anatase TiO_2 nanoparticles are almost uniformly decorated onto the surface of TNTs, forming a peculiar heterogeneous structure of binary composition on nanoscale. The supports/skeletons, TNTs, which possess large specific surface area, are also the precursor of deposited TiO_2 nanoparticles. Thus the heterogeneous structure of TiO_2/TNTs ensures the high photocatalytic activity of TiO_2. Previous work also demonstrated a higher photocatalytic reactivity of TiO_2/TNTs than both TNTs and nano-TiO_2 over acetone (Yu et al., 2007).

3.3. Effect of TiO_2/TNTs dosage on photocatalytic degradation of BPA

Fig. 5 displays the photocatalytic degradation kinetics of BPA at different TiO_2/TNTs dosages. Higher removal efficiency and faster degradation kinetics were observed at higher dosage of the

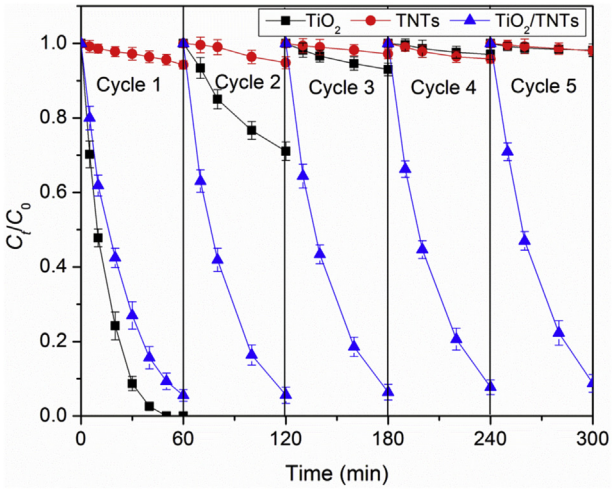

Fig. 3. Photocatalytic degradation of BPA by TiO_2, TNTs and TiO_2/TNTs over 5 continuous cycles (Initial BPA = 5 mg/L, material dosage = 0.2 g/L, initial pH = 7.0 ± 0.2, temperature = 25 ± 2 °C).

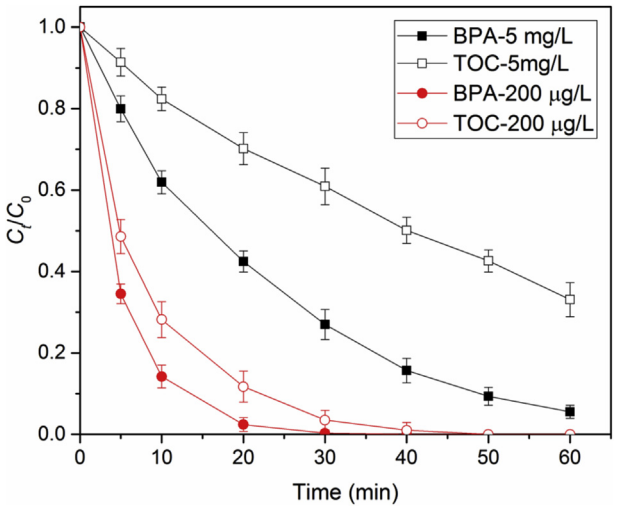

Fig. 4. Photocatalytic degradation of BPA by TiO_2/TNTs at different initial concentrations and mineralization efficiency (Initial BPA = 5 mg/L and 200 μg/L, material dosage = 0.2 g/L, initial pH = 7.0 ± 0.2, temperature = 25 ± 2 °C).

material. Table S5 gives the calculated parameters of the first-order kinetic models. Fairly good model fitting for degradation was obtained for the simplified first-order kinetics model with $R^2 > 0.99$ in all cases. Addition of 0.05 g/L of TiO_2/TNTs only removed 86.1% of BPA with a k_1 of 0.0324 min^{-1}. While the removal efficiency reached up to 97.8% when 0.8 g/L of TiO_2/TNTs added and the removal rate was nearly doubled (0.0635 min^{-1}).

In the present study, the removal efficiency of BPA was enhanced at higher TiO_2/TNTs dosage. Higher dosage of photocatalyst can provide more active sites for BPA reaction due to more radicals production, and the enchantment effect will be limited when the system is saturated (Kaneco et al., 2004; Tsai et al., 2009). It is because excess catalysts cannot enhance the reactivity anymore but shield part of UV illumination resulting in a saturated system, and self-consumption of radicals (·OH in our system) dramatically occur at higher concentration (Andreottola et al., 2008; Kaneco et al., 2004; Tsai et al., 2009). Since high BPA removal efficiency (94.4%) was got at 0.2 g/L, we chose this material dosage in the following tests for economy and cost consideration.

3.4. Effects of water chemistry factors on photocatalytic degradation of BPA by TiO_2/TNTs

3.4.1. Effect of initial pH on photocatalytic degradation of BPA

Fig. 6a shows the kinetics results of BPA photocatalysis by TiO_2/TNTs at initial pH of 3–11. The total removal of BPA was promoted with increasing pH. The first-order apparent removal rate k_1 increased from 0.0301 to 0.0594 min^{-1} when initial pH increased from 3 to 11 (Table S5), implying the BPA photocatalysis by TiO_2/TNTs was more favored under alkaline condition.

Solution pH can play multiple roles during the photocatalytic degradation of BPA (Akpan and Hameed, 2009; Konstantinou and Albanis, 2004). Firstly, the ionization state of BPA and the surface charge of the TiO_2/TNTs are highly pH-dependent. Since photocatalytic oxidation mainly occurs at the surface of photocatalyst (Akpan and Hameed, 2009), the effective surface interactions between photocatalyst and BPA will influence the overall degradation. BPA with a pK_a value of 9.6 (Table S1) can be ionized to bisphenolate anions when pH is higher (Kosky et al., 1991). Meanwhile, the ionization state of TiO_2 or titanate surface is changed followed the reactions (Akpan and Hameed, 2009):

$$\equiv Ti - OH + H^+ \rightarrow \equiv Ti - OH_2^+ \quad (12)$$

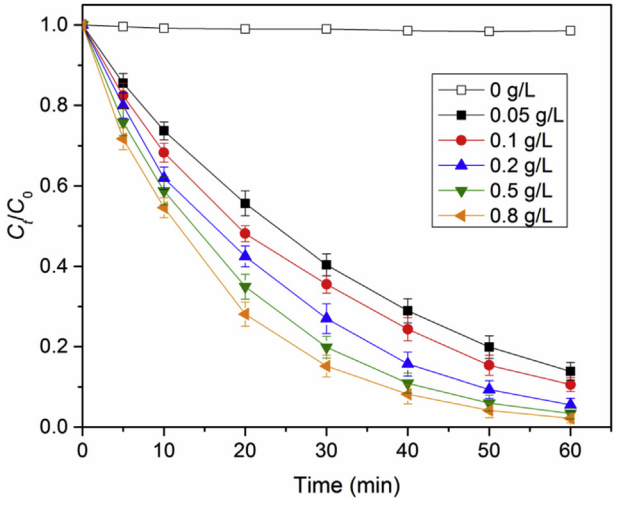

Fig. 5. Effect of material dosage on photocatalytic degradation of BPA by TiO_2/TNTs (Initial BPA = 5 mg/L, pH = 7.0 ± 0.2, temperature = 25 ± 0.5 °C).

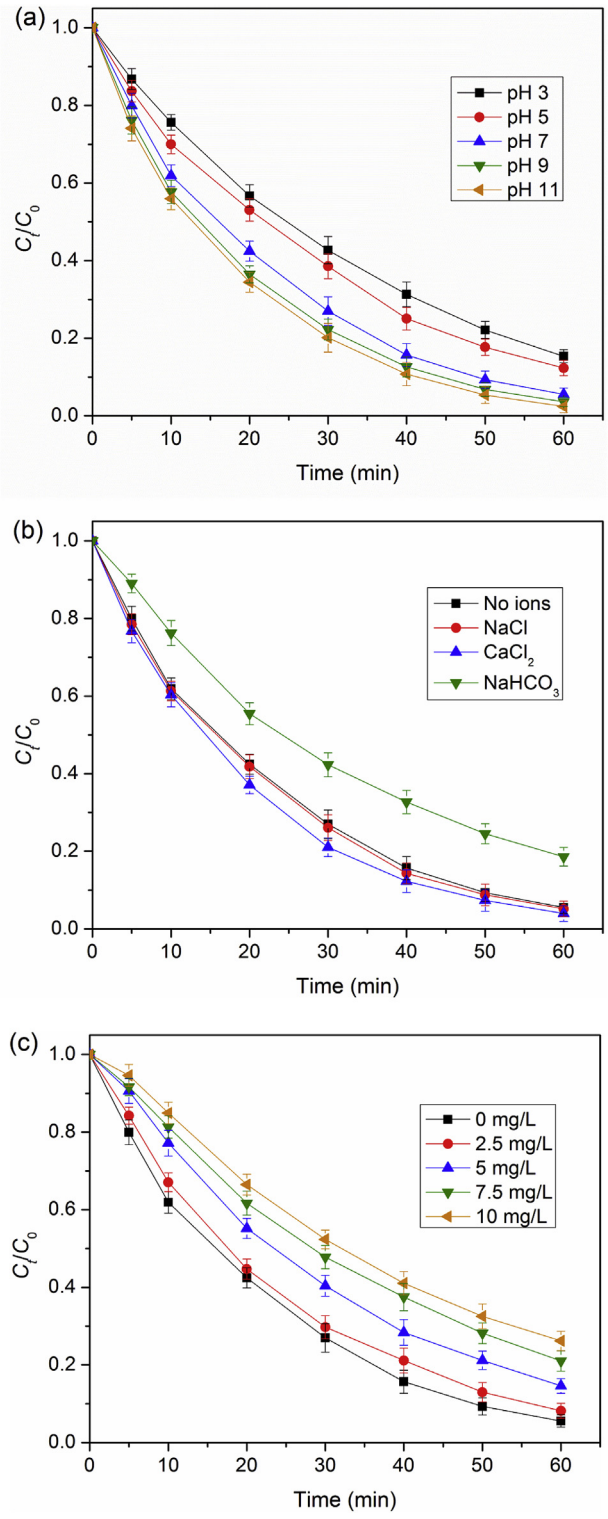

Fig. 6. Effect of **(a)** pH, **(b)** co-existing ions and **(c)** HA on photocatalytic degradation of BPA by TiO_2/TNTs (Initial BPA = 5 mg/L, material dosage = 0.2 g/L, temperature = 25 ± 0.5 °C; for (b) and (c), pH = 7.0 ± 0.2; for (b), ion concentration = 5 mM).

$$\equiv Ti - OH + OH^- \rightarrow \equiv Ti - O^- + H_2O \quad (13)$$

in which "≡Ti" represents the basic lattice structure of TiO_2 and titanate, i.e. [TiO_6] octahedron.

First, at alkaline pH, OH^- will occupy more reactive sites resulting in decreased zeta potentials and negative charge for Ti-based materials (Fig. S4). The detected pH_{PZC} for TiO_2/TNTs is 2.93 (Fig. S4), and TiO_2/TNTs are negatively charged at pH 3 to 11. At pH 9 and 11 the electrostatic repulsion between the bisphenolate anions and TiO_2/TNTs may lead to a suppressed contact frequency and reactivity. A decreasing trend of BPA photodegradation efficiency (removal dropped from 100% to ~90%) under UV by TiO_2 was found at pH 9 to 11 in previous studies, and the researchers suggested the enhanced repulsion due to charge reversal of BPA played the key role (Tsai et al., 2009).

Second, solution pH can also affect the generation of ROS (e.g., ·OH, $\cdot O_2^-$, and H_2O_2) (Akpan and Hameed, 2009; Konstantinou and Albanis, 2004). The positive holes (h^+) and hydroxyl radicals (·OH) are regarded as the major oxidation species under acidic conditions, and neutral or basic conditions, respectively (Akpan and Hameed, 2009; Tunesi and Anderson, 1991). Fast degradation of BPA was observed at pH 2.6 by nano-TiO_2 under solar irradiation while limited hydroxyl radicals were generated implying positive holes or some other ROS (e.g., superoxide radicals) may play the key role (Wu et al., 2016). Since alkaline conditions are more beneficial for ·OH production, an increasing trend for BPA photolysis was reported from neutral to higher pH values in several studies (Kaneco et al., 2004; Wang et al., 2009; Wu et al., 2016).

Third, the aggregation of photocatalyst is affected by pH. The aggregation of photocatalysts can cause great loss of available surface sites for adsorption of target contaminant and photons (Akpan and Hameed, 2009; Fox and Dulay, 1993; Konstantinou and Albanis, 2004). According to previous work, the maximum aggregation of TiO_2/TNTs occurred at around its pH_{PZC} (2.93) (Liu et al., 2013a), which is another reason on the increasing trend of BPA photolysis efficiency by TiO_2/TNTs at pH > 3.

In summary, solution pH governs a) the surface charge of both photocatalysts and target contaminants; b) generation of effective ROS; and c) the aggregation of photocatalysts. Thereby, the overall effect of pH depends on the balance of these three aspects. Therefore, more ROS production and less aggregation at higher pH resulted in the overall increasing trend for BPA photocatalysis from pH 3 to 11.

3.4.2. Effect of coexisting ions on photocatalytic degradation of BPA

Fig. 6b presents the BPA photodegradation kinetics in the presence of various common ions. The addition of 5 mM of NaCl and $CaCl_2$ just slightly increased the BPA removal from 94.4% to 94.8% and 96.0%, respectively, while there is no significant difference according to *t*-tests ($p > 0.05$, level of significance = 0.05). The introduction of 5 mM of $NaHCO_3$ reduced the BPA removal to 81.4% with a slower kinetic, and the difference is statistically significant ($p < 0.05$, level of significance = 0.05) compared to that without any salt addition.

Mechanisms on effects of Na^+ and Ca^{2+} are complicated, as they can affect not only aggregation of photocatalyst but also reaction with BPA. Firstly, both Na^+ and Ca^{2+} can be strongly adsorbed on to TNTs through ion exchange (Liu et al., 2013a, 2013b). Based on the typical Derjaguin-Landau-Verwey-Overbeek (DLVO) theory, addition of Na^+ and Ca^{2+} can induce electrical double layer compression, which is described as the reduced thickness of electrical double layer and suppressed electrostatic repulsion between TNTs (Liu et al., 2013a; Wang et al., 2013). Therefore stabilization is impaired and the aggregation is enhanced at elevated ionic strength. It was reported that the increase of Na^+ or Ca^{2+} addition greatly enhanced the aggregation of TiO_2/TNTs (Liu et al., 2013a). However, based on the observation in this study (Fig. 6b), the greater aggregation at higher Na^+/Ca^{2+}concentrations did not lead to decrease of BPA degradation efficiency. It is because of the promoting effect on BPA removal by addition of Na^+ and Ca^{2+}. This can partially attribute to the "salting-out effect" at higher ionic strength, which can decrease the solubility of BPA enhancing its sorption onto TiO_2/TNTs (Bautista-Toledo et al., 2005). In addition, the adsorbed cations can create a screening effect which favors π−π adsorbate-adsorbent dispersion interactions between BPA and the photocatalyst (Liu et al., 2016a; Stuart et al., 1991), thereby enhancing the adsorption of BPA. Therefore, integration on negative effect caused by material aggregation and positive effect resulting from screening mechanism led to no significant change of BPA degradation with addition of Na^+ and Ca^{2+}. Similarly, previous study on photocatalysis of 2-naphthol with TiO_2 also demonstrated the effect of Na^+ or Ca^{2+} was negligible (Qourzal et al., 2008).

Anions are generally regarded as scavengers of photo-generated holes (h^+) or hydroxyl radicals (Konstantinou and Albanis, 2004). Anion can pose inhibition effects through following reactions (Bhatkhande et al., 2002; Konstantinou and Albanis, 2004):

$$Cl^- + h_{VB}^+ \rightarrow \cdot Cl \quad (14)$$

$$Cl^- + \cdot OH \rightarrow \cdot ClOH^- \quad (15)$$

$$HCO_3^- + \cdot OH \rightarrow \cdot CO_3^- + H_2O \quad (16)$$

$$CO_3^{2-} + \cdot OH \rightarrow \cdot CO_3^- + OH^- \quad (17)$$

The reactivity of produced radical anions (e.g., ·Cl and $\cdot CO_3^-$) are much weaker than h^+ or ·OH (Fukahori et al., 2003a). A previous work using C-N co-doped TiO_2 also demonstrated that chloride at 5 mM only slightly retarded the BPA degradation (removal dropped by ~1%), while bicarbonate (also 5 mM) exhibited a larger extent of inhibition (removal dropped from 100% to 67%) (Wang and Lim, 2010). The researchers pointed out that bicarbonate can be irreversibly adsorbed onto the Ti-based materials, so completive adsorption of HCO_3^- with produced radicals (e.g., ·OH) onto the photocatalyst would inhibit BPA reaction (Hu et al., 2004; Rincon and Pulgarin, 2004; Wang and Lim, 2010). However, the chloride anions can only be loosely attracted to the material surface through hydrogen bridges and Van der Waals force (Hu et al., 2004; Rincon and Pulgarin, 2004; Wang and Lim, 2010). Moreover, bicarbonate can quench the hydroxyl radicals (Eq. (16)) faster than chloride (Gultekin and Ince, 2004). Therefore, the inhibition effect of bicarbonate is more important.

3.4.3. Effect of HA on photocatalytic degradation of BPA

Fig. 6c shows the effect of dissolved HA on the BPA photolysis kinetics at neutral conditions. Addition of HA inhibited the photodegradation of BPA by TiO_2/TNTs. Specifically, as 2.5 mg/L (as TOC) of HA added, the total removal of BPA dropped slightly from 94.4% to 91.8%. However, with more HA introduced, the degradation of BPA was suppressed distinctly. When the HA concentration increased to 10 mg/L, the lowest removal efficiency (73.8%) and k_1 (0.0229 min^{-1}) were obtained.

Adsorption of HA onto TiO_2/TNTs could quickly reach equilibrium within 60 min due to the large surface area of the material (Fig. S6), and Fig. S7 presents the adsorption isotherm of HA by TiO_2/TNTs. The linear isotherm model can well describe ($R^2 = 0.9962$) the adsorption process, with a distribution coefficient (K_d) of 7.04 (M4 in Supplementary data). Therefore, more HA was

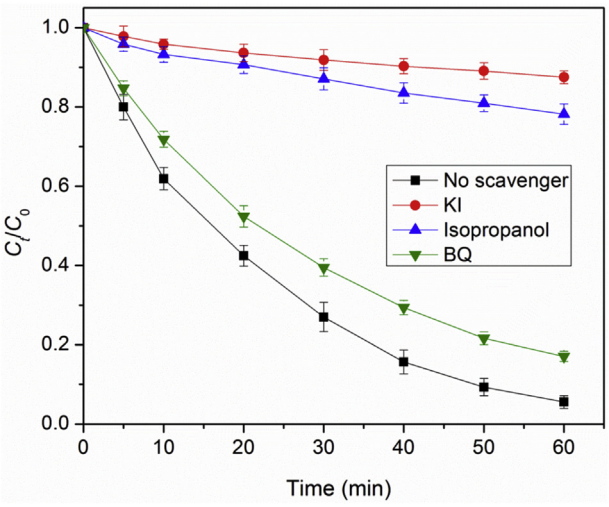

Fig. 7. Photocatalytic degradation of BPA by TiO_2/TNTs in the presence of various radical scavengers. (Initial BPA = 5 mg/L, scavenger concentration = 10 mM, material dosage = 0.2 g/L, pH = 7.0 ± 0.2, temperature = 25 ± 0.5 °C).

adsorbed onto TiO_2/TNTs at higher HA concentration. For example, q_e (29.2 mg/g) at 10 mg/L was much larger than that (7.7 mg/g) at 2.5 mg/L. In this study, HA molecules can exist either on the surface of TiO_2/TNTs or freely in the aqueous phase. These two groups of HA may pose different effects on BPA photodegradation. It has been described that HA molecules can be sorbed onto nano-TiO_2 and titanate through electrostatic attraction or ligand exchange (Chen et al., 2014; Liu et al., 2016b; Ma et al., 2017; Wu et al., 2016). The sorbed HA molecules cause contrasting effects on BPA photolysis. On one hand, higher amount of sorbed HA can reduce the zeta potential, increase the steric repulsion and inhibit the aggregation of TiO_2/TNTs (Liu et al., 2013a; Wu et al., 2016), which are all beneficial for creating larger specific area and more available active sites. Moreover, HA molecules can serve as electron donor to scavenge the photo-generated holes, leading to inhibited electron-hole recombination and enhanced the ·OH generation (Selli et al., 2000). On the other hand, the sorbed HA can also trigger blockage of active sites, surface deactivation or light attenuation resulting in inhibited degradation of BPA (Bekbolet et al., 2002; Konstantinou and Albanis, 2004; Wiszniowski et al., 2002). The freely dissolved HA molecules can also shield the UV illumination since the HA molecules are also strong UV absorber (Selli et al., 2000; Wu et al., 2016).

In a previous work using nano-TiO_2 for BPA photolysis under solar light, researchers observed that the degradation of BPA was enhanced with only 0.1 mg/L of HA added, then impeded with more HA (1 and 10 mg/L) introduced (Wu et al., 2016). However, we did not found similar enhancement of BPA in this study, implying that the addition of HA (≥1 mg/L as TOC) might be oversaturated to cause a facilitation of ·OH generation. In our study, the BPA photodegradation was inhibited with increasing HA concentration, suggesting the aforementioned negative effects of HA surpassed the positive effects in all cases.

3.5. Degradation pathway and DFT calculation

Fig. 7 presents the radical quenching results in the presence of scavengers. KI is for quenching of h^+, isopropanol for ·OH and BQ for $\cdot O_2^-$ (Guo et al., 2013). Addition of isopropanol greatly inhibited the reaction, indicating ·OH played the primary role in BPA degradation. In addition, addition of KI resulted in dramatic decrease on BPA degradation. It is because KI can the prevent formation of h^+, which is highly related to the formation of ·OH according to Eq. (8). However, a slight decrease was found after in the presence of BQ, suggesting $\cdot O_2^-$ did not dominate the photodegradation in this system.

Theoretical DFT method is further used to elucidate the exact photocatalytic degradation pathways of BPA, and the regioselectivity for ·OH attacking is focused. Generally, the highest occupied molecular orbital (HOMO) indicates easy escape of electron, which will be attacked by ·OH with the highest probability (Casida et al., 1998; Pearson, 1986). The HOMO orbital of BPA is mainly located on the symmetrical phenyl rings (Fig. 8b), where can be easily attacked by ·OH. The natural population analysis (NPA) charge distribution and Fukui index representing radical attack (f^0) of carbon atoms in BPA are further calculated (Fig. 8c). The red color degree in Fig. 8c shows different levels of f^0, and it demonstrates that the C4, C4′, C6, and C6' in BPA (marked in pink in Fig. 8a) with high values are the most reactive sites for radical attacks.

Base on the products identified by LC-MS and DFT calculation results, we proposed the BPA degradation pathway (Fig. 9). Compounds A (6,6′-diOH-BPA), E (2-isopropylmuconic acid) and F (4-isopropenylphenol) were the detected intermediates through LC-MS, and therefore photocatalytic degradation of BPA generally undergoes three pathways: 1) BPA→A→D→E, 3) BPA→B/C→D→E and 3) BPA→B/C→F, which is consistent with the precious studies (Guo et al., 2009; Subagio et al., 2010). According

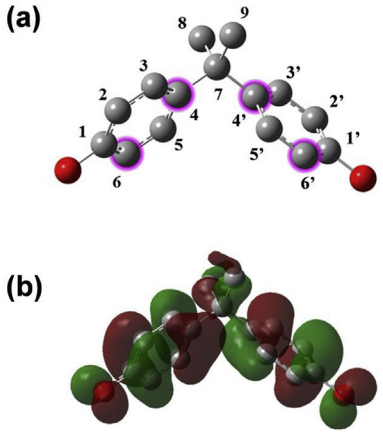

(c)

No.	Atom	Charge (-1) (e/Å^3)	Charge (0) (e/Å^3)	Charge (+1) (e/Å^3)	f^0
1	C	0.182	0.281	0.343	0.081
2	C	-0.230	-0.273	-0.244	-0.007
3	C	-0.240	-0.219	-0.205	0.018
4	C	-0.065	-0.044	0.046	0.056
5	C	-0.251	-0.232	-0.215	0.018
6	C	-0.487	-0.311	-0.259	0.114
7	C	-0.115	-0.112	-0.127	-0.006
8	C	-0.687	-0.695	-0.700	-0.006
9	C	-0.687	-0.695	-0.700	-0.006

Fig. 8. **(a)** BPA chemical structure; **(b)** HOMO orbital of BPA; **(c)** NPA charge distribution and Fukui index of BPA.

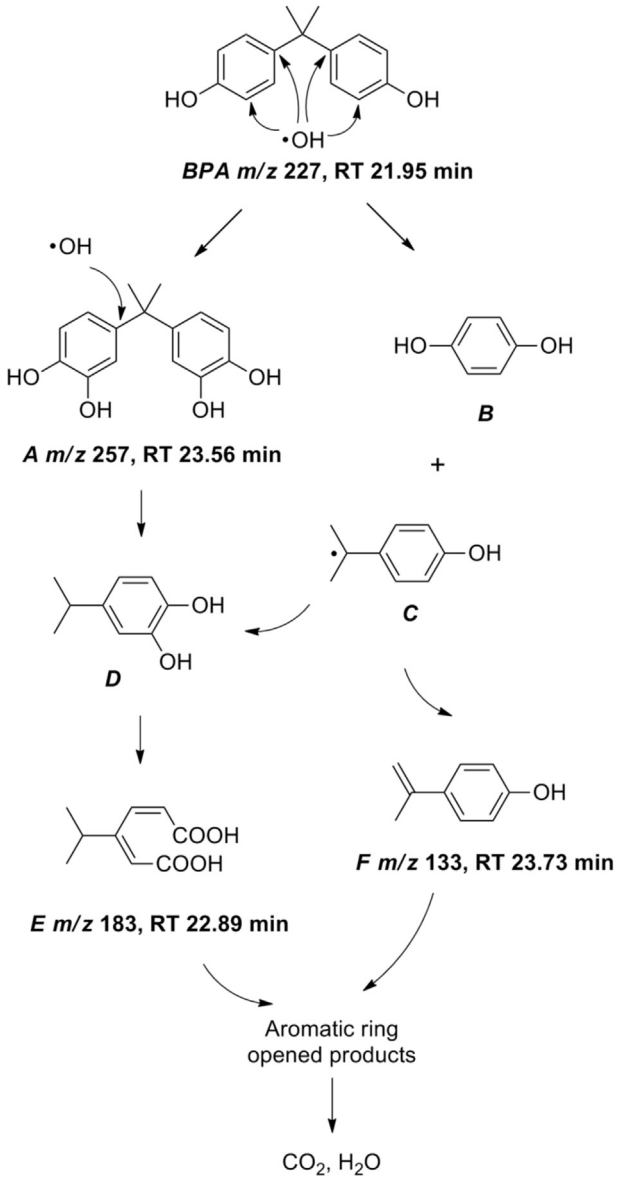

Fig. 9. Proposed BPA degradation pathway by TiO_2/TNTs under UV light.

to DFT calculation results, the hydroxyl radicals prefer to attack on C6 and C6′, resulting in 6,6′-diOH-BPA (A, *m/z* 257) formation. In the meanwhile, ·OH radical attacking on C4 or C4′ will lead to breakage of C4–C7 bond, and formation of 1,4-hydroquinone (B) and transient radical ($^*C(CH_3)_2C_6H_4OH$, C). Then the $^*C(CH_3)_2C_6H_4OH$ will soon transform into the stable 4-isopropenylphenol (F, *m/z* 133). In addition, the hydroxylation of aromatic ring by hydroxyl radicals can lead to the sequential ring cleavage. The attacks of hydroxyl radical on A and C may produce the same intermediate D, which can then form 2-isopropylmuconic acid (E, *m/z* 183) after a ring-open process. The ring-opened products will be further oxidized by ·OH to form aliphatic compounds (e.g., carboxylic acids, formic acid and acetic acid) and final mineralization products of CO_2 and H_2O (Guo et al., 2009; Subagio et al., 2010), which is consistent with the TOC elimination shown in Fig. 4.

4. Conclusions

This study developed and tested a TiO_2 decorated TNTs (TiO_2/TNTs) for photocatalytic degradation of BPA under UV irradiation. The primary findings are summarized as:

(1) The synthesized TiO_2/TNTs is a nano composite of anatase and titanate, of which anatase serves as primary photocatalyst and titanate as the skeleton/support. The heterogeneous structure of TiO_2/TNTs ensures high photocatalytic activity under UV light.
(2) TiO_2/TNTs exhibited excellent photocatalytic reactivity for BPA over 5 cycles. 95.8% of TiO_2/TNTs could be separated through gravity-settling. As high as 91.2% of BPA also could be degraded by TiO_2/TNTs in the 5th cycle, which was much higher than that by virgin TiO_2 (1.8%) and TNTs (2.0%).
(3) Influences of typical water chemistry parameters on BPA photodegradation were tested. Higher pH facilitated photocatalysis due to more ROS produced and less material aggregation. Co-existing NaCl and $CaCl_2$ showed negligible effects on BPA degradation, but $NaHCO_3$ caused an inhibition effect resulting from consumption of ·OH. HA inhibited degradation mainly due to blockage of the photocatalyst's active sites.
(4) Hydroxyl radicals play the dominate role in BPA photocatalytic degradation. DFT theory is used to interpret the BPA degradation pathway. High Fukui index considering radical attack (f^0) indicates that the easy-attacking sites on BPA are carbon atoms on the symmetrical phenyl rings.

Overall, TiO_2/TNTs would be a promising photocatalyst for BPA removal from wastewaters through photocatalysis, and the theoretical calculation presented in this study also provides an available way for research on organic compounds degradation mechanism. Moreover, considering the good adsorption capacity of TNTs for heavy metal cations (Bavykin et al., 2006; Liu et al., 2013b, 2016b), TiO_2/TNTs also show a great application potential in the organics-heavy metals combined contaminants remediation area.

Acknowledgements

Financially supported from the National Natural Science Foundation of China (grant No. 51508006) is much appreciated. Dr. Xiao Zhao is grateful for the support by General Financial Grant from the China Postdoctoral Science Foundation (grant No. 2016M601056). Dr. Jie Fu is thankful to Fudan University for the financial support (grant no. JIH1829022).

Appendix A. Supplementary data

Supplementary data related to this article can be found at https://doi.org/10.1016/j.envpol.2017.09.094.

References

Akbari, S., Ghanbari, F., Moradi, M., 2016. Bisphenol A degradation in aqueous solutions by electrogenerated ferrous ion activated ozone, hydrogen peroxide and persulfate: applying low current density for oxidation mechanism. Chem. Eng. J. 294, 298–307.
Akpan, U., Hameed, B., 2009. Parameters affecting the photocatalytic degradation of dyes using TiO_2-based photocatalysts: a review. J. Hazard. Mater 170, 520–529.
Anderson, C., Bard, A.J., 1997. Improved photocatalytic activity and characterization of mixed TiO_2/SiO_2 and TiO_2/Al_2O_3 materials. J. Phys. Chem. B 101, 2611–2616.
Andreottola, G., Dallago, L., Ferrarese, E., 2008. Feasibility study for the remediation of groundwater contaminated by organolead compounds. J. Hazard. Mater 156, 488–498.
Bautista-Toledo, I., Ferro-Garcia, M., Rivera-Utrilla, J., Moreno-Castilla, C., Vegas Fernández, F., 2005. Bisphenol A removal from water by activated carbon. Effects of carbon characteristics and solution chemistry. Environ. Sci. Technol. 39, 6246–6250.
Bavykin, D.V., Friedrich, J.M., Walsh, F.C., 2006. Protonated titanates and TiO_2 nanostructured materials: synthesis, properties, and applications. Adv. Mater

18, 2807–2824.
Bavykin, D.V., Walsh, F.C., 2010. Titanate and Titania Nanotubes: Synthesis, Properties and Applications. Royal Society of Chemistry, Cambridge, MA, UK.
Bekbolet, M., Suphandag, A.S., Uyguner, C.S., 2002. An investigation of the photocatalytic efficiencies of TiO_2 powders on the decolourisation of humic acids. J. Photoch. Photobio. A Chem. 148, 121–128.
Bhatkhande, D.S., Pangarkar, V.G., Beenackers, A.A., 2002. Photocatalytic degradation for environmental applications–a review. J. Chem. Technol. Biotechnol. 77, 102–116.
Brunauer, S., Deming, L.S., Deming, W.E., Teller, E., 1940. On a theory of the van der Waals adsorption of gases. J. Am. Chem. Soc. 62, 1723–1732.
Cai, Y., Strømme, M., Welch, K., 2013. Photocatalytic antibacterial effects are maintained on resin-based TiO_2 nanocomposites after cessation of UV irradiation. PLoS One 8, e75929.
Casida, M.E., Jamorski, C., Casida, K.C., Salahub, D.R., 1998. Molecular excitation energies to high-lying bound states from time-dependent density-functional response theory: characterization and correction of the time-dependent local density approximation ionization threshold. J. Chem. Phys. 108, 4439–4449.
Cates, E.L., 2017. Photocatalytic water treatment: so where are we going with this? Environ. Sci. Technol. 51, 757–758.
Chen, H.Y., Lo, S.L., Ou, H.H., 2013. Catalytic hydrogenation of nitrate on Cu–Pd supported on titanate nanotube and the experiment after aging, sulfide fouling and regeneration procedures. Appl. Catal. B Environ. 142, 65–71.
Chen, Q., Zhou, W., Du, G., Peng, L.M., 2002. Trititanate nanotubes made via a single alkali treatment. Adv. Mater 14, 1208–1211.
Chen, W., Qian, C., Liu, X.Y., Yu, H.Q., 2014. Two-dimensional correlation spectroscopic analysis on the interaction between humic acids and TiO_2 nanoparticles. Environ. Sci. Technol. 48, 11119–11126.
Di Valentin, C., Finazzi, E., Pacchioni, G., Selloni, A., Livraghi, S., Czoska, A., Paganini, M., Giamello, E., 2008. Density functional theory and electron paramagnetic resonance study on the effect of N-F codoping of TiO_2. Chem. Mater 20, 3706–3714.
Doong, R.-a., Liao, C.-Y., 2016. Enhanced visible-light-responsive photodegradation of bisphenol A by Cu, N-codoped titanate nanotubes prepared by microwave-assisted hydrothermal method. J. Hazard. Mater 332, 254–262.
Flint, S., Markle, T., Thompson, S., Wallace, E., 2012. Bisphenol A exposure, effects, and policy: a wildlife perspective. J. Environ. Manage 104, 19–34.
Fox, M.A., Dulay, M.T., 1993. Heterogeneous photocatalysis. Chem. Rev. 93, 341–357.
Frisch, M.J., Trucks, G.W., Schlegel, H.B., Scuseria, G.E., Robb, M.A., Cheeseman, J.R., Montgomery, J.A., Vreven, T., Kudin, K.N., Burant, J.C., Millam, J.M., Iyengar, S.S., Tomasi, J., Barone, V., Mennucci, B., Cossi, M., Scalmani, G., Rega, N., Petersson, G.A., Nakatsuji, H., Hada, M., Ehara, M., Toyota, K., Fukuda, R., Hasegawa, J., Ishida, M., Nakajima, T., Honda, Y., Kitao, O., Nakai, H., Klene, M., Li, X., Knox, J.E., Hratchian, H.P., Cross, J.B., Bakken, V., Adamo, C., Jaramillo, J., Gomperts, R., Stratmann, R.E., Yazyev, O., Austin, A.J., Cammi, R., Pomelli, C., Ochterski, J.W., Ayala, P.Y., Morokuma, K., Voth, G.A., Salvador, P., Dannenberg, J.J., Zakrzewski, V.G., Dapprich, S., Daniels, A.D., Strain, M.C., Farkas, O., Malick, D.K., Rabuck, A.D., Raghavachari, K., Foresman, J.B., Ortiz, J.V., Cui, Q., Baboul, A.G., Clifford, S., Cioslowski, J., Stefanov, B.B., Liu, G., Liashenko, A., Piskorz, P., Komaromi, I., Martin, R.L., Fox, D.J., Keith, T., Laham, A., Peng, C.Y., Nanayakkara, A., Challacombe, M., Gill, P.M.W., Johnson, B., Chen, W., Wong, M.W., Gonzalez, C., Pople, J.A., 2003. Gaussian 03, Revision C.02.
Fromme, H., Küchler, T., Otto, T., Pilz, K., Müller, J., Wenzel, A., 2002. Occurrence of phthalates and bisphenol A and F in the environment. Water Res. 36, 1429–1438.
Fukahori, S., Ichiura, H., Kitaoka, T., Tanaka, H., 2003a. Capturing of bisphenol A photodecomposition intermediates by composite TiO_2-zeolite sheets. Appl. Catal. B Environ. 46, 453–462.
Fukahori, S., Ichiura, H., Kitaoka, T., Tanaka, H., 2003b. Photocatalytic decomposition of bisphenol A in water using composite TiO_2-zeolite sheets prepared by a papermaking technique. Environ. Sci. Technol. 37, 1048–1051.
Grandcolas, M., Cottineau, T., Louvet, A., Keller, N., Keller, V., 2013. Solar light-activated photocatalytic degradation of gas phase diethylsulfide on WO_3-modified TiO_2 nanotubes. Appl. Catal. B Environ. 138, 128–140.
Gultekin, I., Ince, N.H., 2004. Degradation of reactive azo dyes by UV/H_2O_2: impact of radical scavengers. J. Environ. Sci. Heal. A 39, 1069–1081.
Gültekin, I., Ince, N.H., 2007. Synthetic endocrine disruptors in the environment and water remediation by advanced oxidation processes. J. Environ. Manage 85, 816–832.
Guo, C., Ge, M., Liu, L., Gao, G., Feng, Y., Wang, Y., 2009. Directed synthesis of mesoporous TiO_2 microspheres: catalysts and their photocatalysis for bisphenol A degradation. Environ. Sci. Technol. 44, 419–425.
Guo, C., Xu, J., Wang, S., Zhang, Y., He, Y., Li, X., 2013. Photodegradation of sulfamethazine in an aqueous solution by a bismuth molybdate photocatalyst. Catal. Sci. Technol. 3, 1603–1611.
Hu, C., Yuchao, T., Lanyu, L., Zhengping, H., Yizhong, W., Hongxiao, T., 2004. Effects of inorganic anions on photoactivity of various photocatalysts under different conditions. J. Chem. Technol. Biotechnol. 79, 247–252.
Kaneco, S., Rahman, M.A., Suzuki, T., Katsumata, H., Ohta, K., 2004. Optimization of solar photocatalytic degradation conditions of bisphenol A in water using titanium dioxide. J. Photoch. Photobio. A Chem. 163, 419–424.
Kondrakov, A., Ignatev, A., Frimmel, F., Bräse, S., Horn, H., Revelsky, A., 2014. Formation of genotoxic quinones during bisphenol A degradation by TiO_2 photocatalysis and UV photolysis: a comparative study. Appl. Catal. B Environ. 160, 106–114.
Konstantinou, I.K., Albanis, T.A., 2004. TiO_2-assisted photocatalytic degradation of azo dyes in aqueous solution: kinetic and mechanistic investigations: a review. Appl. Catal. B Environ. 49, 1–14.
Kosky, P.G., Silva, J.M., Guggenheim, E.A., 1991. The aqueous phase in the interfacial synthesis of polycarbonates. Part 1. Ionic equilibria and experimental solubilities in the BPA-sodium hydroxide-water system. Ind. Eng. Chem. Res. 30, 462–467.
Lee, C.K., Wang, C.C., Lyu, M.D., Juang, L.C., Liu, S.S., Hung, S.H., 2007. Effects of sodium content and calcination temperature on the morphology, structure and photocatalytic activity of nanotubular titanates. J. Colloid Interface Sci. 316, 562–569.
Liu, W., Cai, Z., Zhao, X., Wang, T., Li, F., Zhao, D., 2016a. High-capacity and photo-regenerable composite material for efficient adsorption and degradation of phenanthrene in water. Environ. Sci. Technol. 50, 11174–11183.
Liu, W., Ni, J., Yin, X., 2014. Synergy of photocatalysis and adsorption for simultaneous removal of Cr(VI) and Cr(III) with TiO_2 and titanate nanotubes. Water Res. 53, 12–25.
Liu, W., Sun, W., Borthwick, A.G., Ni, J., 2013a. Comparison on aggregation and sedimentation of titanium dioxide, titanate nanotubes and titanate nanotubes-TiO_2: influence of pH, ionic strength and natural organic matter. Colloid. Surf. A 434, 319–328.
Liu, W., Wang, T., Borthwick, A.G., Wang, Y., Yin, X., Li, X., Ni, J., 2013b. Adsorption of Pb^{2+}, Cd^{2+}, Cu^{2+} and Cr^{3+} onto titanate nanotubes: competition and effect of inorganic ions. Sci. Total. Environ. 456, 171–180.
Liu, W., Zhao, X., Borthwick, A.G., Wang, Y., Ni, J., 2015. Dual-enhanced photocatalytic activity of Fe-deposited titanate nanotubes used for simultaneous removal of As(III) and As(V). ACS Appl. Mater. Interfaces 7, 19726–19735.
Liu, W., Zhao, X., Wang, T., Zhao, D., Ni, J., 2016b. Adsorption of U(VI) by multilayer titanate nanotubes: effects of inorganic cations, carbonate and natural organic matter. Chem. Eng. J. 286, 427–435.
Lombó, M., Fernández-Díez, C., González-Rojo, S., Navarro, C., Robles, V., Herráez, M.P., 2015. Transgenerational inheritance of heart disorders caused by paternal bisphenol A exposure. Environ. Pollut. 206, 667–678.
Ma, J., Li, F., Qian, T., Liu, H., Liu, W., Zhao, D., 2017. Natural organic matter resistant powder activated charcoal supported titanate nanotubes for adsorption of Pb(II). Chem. Eng. J. 315, 191–200.
Mutin, P.H., Lafond, V., Popa, A.F., Granier, M., Markey, L., Dereux, A., 2004. Selective surface modification of SiO_2-TiO_2 supports with phosphonic acids. Chem. Mater 16, 5670–5675.
Ohko, Y., Ando, I., Niwa, C., Tatsuma, T., Yamamura, T., Nakashima, T., Kubota, Y., Fujishima, A., 2001. Degradation of bisphenol A in water by TiO_2 photocatalyst. Environ. Sci. Technol. 35, 2365–2368.
Parr, R.G., Yang, W.T., 1984. Density functional-approach to the frontier-electron theory of chemical-reactivity. J. Am. Chem. Soc. 106, 4049–4050.
Pearson, R.G., 1986. Absolute electronegativity and hardness correlated with molecular orbital theory. P. Natl. Acad. Sci. 83, 8440–8441.
Qourzal, S., Barka, N., Tamimi, M., Assabbane, A., Ait-Ichou, Y., 2008. Photodegradation of 2-naphthol in water by artificial light illumination using TiO_2 photocatalyst: identification of intermediates and the reaction pathway. Appl. Catal. A Gen. 334, 386–393.
Rincon, A.-G., Pulgarin, C., 2004. Effect of pH, inorganic ions, organic matter and H_2O_2 on *E. coli* K12 photocatalytic inactivation by TiO_2: implications in solar water disinfection. Appl. Catal. B Environ. 51, 283–302.
Rogers, J.A., Metz, L., Yong, V.W., 2013. Review: endocrine disrupting chemicals and immune responses: a focus on bisphenol-A and its potential mechanisms. Mol. Immunol. 53, 421–430.
Satterfield, C.N., 1970. Mass Transfer in Heterogeneous Catalysis. MIT Press, Cambridge, MA, UK.
Selli, E., Eliet, V., Spini, M.R., Bidoglio, G., 2000. Effects of humic acids on the photoinduced reduction of U(VI) in the presence of semiconducting TiO_2 particles. Environ. Sci. Technol. 34, 3742–3748.
Sheng, G., Yang, S., Sheng, J., Zhao, D., Wang, X., 2011. Influence of solution chemistry on the removal of Ni(II) from aqueous solution to titanate nanotubes. Chem. Eng. J. 168, 178–182.
Staples, C.A., Dome, P.B., Klecka, G.M., Oblock, S.T., Harris, L.R., 1998. A review of the environmental fate, effects, and exposures of bisphenol A. Chemosphere 36, 2149–2173.
Stuart, M.C., Fleer, G., Lyklema, J., Norde, W., Scheutjens, J., 1991. Adsorption of ions, polyelectrolytes and proteins. Sci. Adv. Colloid Interface Sci. 34, 477–535.
Subagio, D.P., Srinivasan, M., Lim, M., Lim, T.T., 2010. Photocatalytic degradation of bisphenol-A by nitrogen-doped TiO_2 hollow sphere in a vis-LED photoreactor. Appl. Catal. B Environ. 95, 414–422.
Sun, X., Li, Y., 2003. Synthesis and characterization of ion-exchangeable titanate nanotubes. Chem. Eur. J. 9, 2229–2238.
Thurman, E.M., 2012. Organic Geochemistry of Natural Waters. Springer Science & Business Media.
Torimoto, T., Okawa, Y., Takeda, N., Yoneyama, H., 1997. Effect of activated carbon content in TiO_2-loaded activated carbon on photodegradation behaviors of dichloromethane. J. Photoch. Photobio. A Chem. 103, 153–157.
Tsai, W.T., Lee, M.K., Su, T.Y., Chang, Y.M., 2009. Photodegradation of bisphenol-A in a batch TiO_2 suspension reactor. J. Hazard. Mater 168, 269–275.
Tunesi, S., Anderson, M., 1991. Influence of chemisorption on the photodecomposition of salicylic acid and related compounds using suspended titania ceramic membranes. J. Phys. Chem. 95, 3399–3405.
Vandenberg, L.N., Colborn, T., Hayes, T.B., Heindel, J.J., Jacobs Jr., D.R., Lee, D.-H.,

Shioda, T., Soto, A.M., vom Saal, F.S., Welshons, W.V., 2012. Hormones and endocrine-disrupting chemicals: low-dose effects and nonmonotonic dose responses. Endocr. Rev. 33, 378–455.
Wang, R., Ren, D., Xia, S., Zhang, Y., Zhao, J., 2009. Photocatalytic degradation of Bisphenol A (BPA) using immobilized TiO_2 and UV illumination in a horizontal circulating bed photocatalytic reactor (HCBPR). J. Hazard. Mater 169, 926–932.
Wang, T., Liu, W., Xiong, L., Xu, N., Ni, J., 2013. Influence of pH, ionic strength and humic acid on competitive adsorption of Pb(II), Cd(II) and Cr(III) onto titanate nanotubes. Chem. Eng. J. 215, 366–374.
Wang, X., Lim, T.T., 2010. Solvothermal synthesis of C-N codoped TiO_2 and photocatalytic evaluation for bisphenol A degradation using a visible-light irradiated LED photoreactor. Appl. Catal. B Environ. 100, 355–364.
Wei, J., Sun, W., Pan, W., Yu, X., Sun, G., Jiang, H., 2017. Comparing the effects of different oxygen-containing functional groups on sulfonamides adsorption by carbon nanotubes: experiments and theoretical calculation. Chem. Eng. J. 312, 167–179.
Wiszniowski, J., Robert, D., Surmacz-Gorska, J., Miksch, K., Weber, J.-V., 2002. Photocatalytic decomposition of humic acids on TiO_2: Part I: discussion of adsorption and mechanism. J. Photoch. Photobio. A Chem. 152, 267–273.
Wright-Walters, M., Volz, C., Talbott, E., Davis, D., 2011. An updated weight of evidence approach to the aquatic hazard assessment of bisphenol A and the derivation a new predicted no effect concentration (PNEC) using a non-parametric methodology. Sci. Total. Environ. 409, 676–685.
Wu, W., Shan, G., Wang, S., Zhu, L., Yue, L., Xiang, Q., Zhang, Y., Li, Z., 2016. Environmentally relevant impacts of nano-TiO_2 on abiotic degradation of bisphenol A under sunlight irradiation. Environ. Pollut. 216, 166–172.
Xiong, L., Yang, Y., Mai, J., Sun, W., Zhang, C., Wei, D., Chen, Q., Ni, J., 2010. Adsorption behavior of methylene blue onto titanate nanotubes. Chem. Eng. J. 156, 313–320.
Yu, H., Yu, J., Cheng, B., Lin, J., 2007. Synthesis, characterization and photocatalytic activity of mesoporous titania nanorod/titanate nanotube composites. J. Hazard. Mater 147, 581–587.
Yu, H., Yu, J., Cheng, B., Zhou, M., 2006a. Effects of hydrothermal post-treatment on microstructures and morphology of titanate nanoribbons. J. Solid State Chem. 179, 349–354.
Yu, J., Yu, H., Cheng, B., Trapalis, C., 2006b. Effects of calcination temperature on the microstructures and photocatalytic activity of titanate nanotubes. J. Mol. Catal. A-Chem. 249, 135–142.
Zhang, Y., Zhou, J.L., 2008. Occurrence and removal of endocrine disrupting chemicals in wastewater. Chemosphere 73, 848–853.
Zhao, X., Cai, Z., Wang, T., O'Reilly, S., Liu, W., Zhao, D., 2016a. A new type of cobalt-deposited titanate nanotubes for enhanced photocatalytic degradation of phenanthrene. Appl. Catal. B Environ. 187, 134–143.
Zhao, X., Liu, W., Cai, Z., Han, B., Qian, T., Zhao, D., 2016b. An overview of preparation and applications of stabilized zero-valent iron nanoparticles for soil and groundwater remediation. Water Res. 100, 245–266.
Zhao, Z., Liu, Q., 2007. Mechanism of higher photocatalytic activity of anatase TiO_2 doped with nitrogen under visible-light irradiation from density functional theory calculation. J. Phys. D. Appl. Phys. 41, 025105.
Zhu, H., Gao, X., Lan, Y., Song, D., Xi, Y., Zhao, J., 2004. Hydrogen titanate nanofibers covered with anatase nanocrystals: a delicate structure achieved by the wet chemistry reaction of the titanate nanofibers. J. Am. Chem. Soc. 126, 8380–8381.